Korean J. Chem. Eng., 38(11), 2229-2234 (2021)
DOI: 10.1007/s11814-021-0909-y

pISSN: 0256-1115
eISSN: 1975-7220

Enhanced stability of PdPtAu alloy catalyst for formic acid oxidation

Won Suk Jung*,,† and Jonghee Han***,†**

*School of Food Biotechnology and Chemical Engineering, Hankyong National University, Anseong 17579, Korea
**Research Center of Chemical Technology, Hankyong National University,
327 Jungang-ro, Anseong-si, Gyeonggi-do, 17579, Korea
***Center for Hydrogen-Fuel Cell Research, Korea Institute of Science and Technology,
Hwarang-ro 14-gil 5, Seongbuk-gu, Seoul 02792, Korea
(*Received 15 April 2021 • Revised 6 July 2021 • Accepted 20 July 2021*)

Abstract−In this study, the ternary catalyst, PdPtAu, was synthesized for the electrochemical formic acid oxidation reaction. The catalyst was prepared through the co-precipitation using $NaBH_4$ as a reducing agent. The status of catalyst formation and the extent of average particle size were known by X-ray diffraction (XRD) and transmission electron microscopy (TEM). For this work, we accomplished electrochemical analyses for the PdPtAu, Pd, Pt, and Au, which defines each activity for formic acid oxidation. In durability tests, half cell and single cell tests show even better stability than the Pd and Au catalysts. Stripping tests were carried out after durability tests. Based on results, the ternary PdPtAu catalyst is less deactivated than the Pd, while the catalyst shows higher activity than the Pt. The PdPtAu catalyst represents high resistance for poisoning as compared to the Pd. We demonstrate the stability of the PdPtAu catalyst in the 3-electrode electrochemical system and single cell tests. After 2 h-operation, the deactivation degree of PdPtAu shows 27% loss of the initial current density, while Pd and Pt catalysts lost 39% and 57% of them, respectively.

Keywords: Trimetallic Alloy Catalyst, Formic Acid, Electro-oxidation Reaction, Membrane Electrode Assemblies, Stability

INTRODUCTION

Fuel cells have received great attention over the past few decades because of low greenhouse gas emissions, easy scale-up, and distributed power generation. Among them, direct formic acid fuel cells (DFAFCs) are promising due to human safety, low fuel crossover flux through Nafion®, high energy conversion efficiency, and low oxidation potential [1-8]. The features mentioned above have an advantage over the direct methanol fuel cells or direct ethanol fuel cells.

Pd is known as the most active oxidation catalyst for the formic acid electrochemically. However, the high cost and low stability of the Pd catalyst restrain the commercialization of DFAFCs. Formic acid oxidation follows a dual pathway mechanism. The first pathway is directly oxidized to CO_2, while the other one is indirectly oxidized by way of CO and further oxidized to CO_2 as follows:

$$HCOOH \rightarrow CO_2 + 2H^+ + 2e^- \quad (1)$$

$$HCOOH \rightarrow H_2O + CO_{ads} \rightarrow CO_2 + 2H^+ + 2e^- \quad (2)$$

It is generally believed that CO formed in the indirect pathway is regarded as poisoning species for metallic catalysts such as Pt and Pd, which limits the stability of a catalyst. To enhance CO tolerance and stability, many efforts have focused on Pd-based alloy catalysts, such as PdAu [9-11], PdAg [12,13], PdBi [14,15], PdCo [16-18], PdNi [19,20] and so on. Kivrak et al. investigated the activity of Pd-based bimetallic catalysts alloyed with different transition metals such as Zn, Co, Mn, and V by using $NaBH_4$ [21]. Their results showed that $Pd_{50}Co_{50}$/CNT represented the highest specific and mass activity. Alloy catalysts with different molar ratios of Pd to Bi using ascorbic acid and polyvinylpyrrolidone were reported [15]. The Pd_1Bi_1 catalyst exhibited larger ESCAs, higher activity, and stability for the formic acid oxidation than the commercial Pd/C. Its mass activity was 1.44 A mg^{-1} equivalent to ca. 5-fold higher activity than the commercial Pd/C. Wang et al. synthesized branched PdAu nanowires on graphene by a co-reduction method with poly(diallyldimethyl-ammonium chloride) [9]. The catalyst showed lower onset potential and higher CO resistance than Pd/C for formic acid oxidation. They claimed that the structure enhanced electron transport, specific surface area, and conductivity. Additionally, Au improved the adsorption of OH_{ads} and CO resistance on the catalyst surface. Pd_3Au/C prepared by chemical reduction was reported to investigate the effect of surface segregation of Pd [11]. The Pd surface composition was varied as a function of heat-treatment conditions. The CO-induced Pd_3Au/C, which showed 80% Pd on the catalyst surface, exhibited enhanced electrochemical performance and stability as compared to using the air-induced one. It is attributed to the rearrangement of Pd and Au atoms, resulting in changes in the structure and composition on the catalyst surface stimulated by CO heat treatment. Nanoporous (NP) PdPt alloy was synthesized by the selective dealloying of Al from PdPtAl [22]. It was observed that the performance of the NP-PdPt catalyst (~1.29 A mg^{-1}) outperformed the commercial Pd/C catalyst (~0.6 A mg^{-1}). They asserted that the NP-PdPt catalyst exhibited low formic acid oxidation peak potential (~0.36 V) as compared to Pd and Pt catalysts. The mass activity of NP-PdPt catalysts was approximately threefold higher than that of Pt/C.

†To whom correspondence should be addressed.
E-mail: jungw@hknu.ac.kr, jhan@kist.re.kr

Recent literature reports the advantage of the second metal addition on the catalytic activity by the third body effect [23]. It may cause the composition and electronic properties of catalyst surfaces to lead to enhanced catalytic properties. In this study, we investigated the trimetallic PdPtAu catalyst for the formic acid electrooxidation reaction. The catalysts were analyzed by X-ray diffraction (XRD), transmission electron microscopy (TEM), and electrochemical techniques for performance and stability.

EXPERIMENTAL

1. Synthesis of Catalysts

The trimetallic PdPtAu catalyst was synthesized at the molar ratio of Pd : Pt : Au=4 : 4 : 2 using a wet chemical reduction method. For example, the trimetallic PdPtAu catalyst was synthesized using the chloroplatinic acid solution (Aldrich), tetrachloroauric acid (Aldrich), and palladium dichloride (Aldrich) as precursors. First, the precursors were dissolved in deionized (DI) water at room temperature. An excessive amount of $NaBH_4$ (Sigma-Aldrich) as a reducing agent was added to the mixed solution. The mixture remained in the air overnight to complete precipitation. The precipitate in suspension was washed with DI water three times and dried in the forced convection oven at 95 °C.

2. Characterization

The structural formation of the prepared catalyst was analyzed by XRD and the size of the catalyst was characterized by TEM. XRD analyses were accomplished using a Rigaku D/MAX-2500 X-ray diffractometer operating with the Cu Kα radiation generated at 30 kV and 100 mA at the scan rate of 5.0° min^{-1} between 20-90°. To evaluate the particle size of catalysts, the following Scherrer equation was employed:

$$D = \frac{k\lambda}{10B\cos\theta}$$

where D is the particle size in nm, k is a coefficient taken here as 0.9, λ is the wavelength of X-ray (0.15404 nm), B is the line broadening at half the maximum intensity in radians. And θ is the angle at the position of the maximum peak known as the Bragg angle.

A potentiostat (Solartron 1286) and a conventional three-electrode electrochemical cell were used to investigate the electrochemical properties of the catalysts at ambient temperature. A silver/silver chloride (Ag/AgCl, Gamry) electrode in saturated potassium chloride (KCl) solution and the Pt mesh (Alfa Aesar) were used as a reference electrode and a counter electrode, respectively. The catalyst inks were prepared by ultrasonically mixing an adequate amount of DI water and 5% Nafion® solution (Solution Technology, Inc.). A 5 µl of the ink solution was deposited on the glassy carbon and fully dried. Pd black (Aldrich), Pt black (Johnson Matthey), and Au nano-powder (Aldrich) also were used as working electrodes. While all the solutions were stirred purging with nitrogen, cyclic voltammetry (CV) was performed by sweeping potential from −0.22 and 1.0 V vs. Ag/AgCl and CAs had been measured for 2 h in 5 M HCOOH at constant 0.1 V. Subsequently, stripping tests were performed to observe poisoned electrodes. Every CV and stripping test was carried out at a scan rate of 20 mV s^{-1}. All potential values in this study are vs. Ag/AgCl.

3. Single Cell Tests

Membrane electrode assemblies (MEAs) were fabricated using a direct paint technique as described elsewhere. The active area was 9 cm^2. The catalyst inks were prepared by dispersing the catalyst powders into appropriate amounts of DI water and 5% recast Nafion® solution. Then both the anode and cathode catalyst inks were directly painted onto either side of the Nafion® 115 membrane. A commercially Pt black was used for the cathode catalyst layer at a loading of 7 mg cm^{-2}, while the loading of anode catalysts on the membrane was 8 mg cm^{-2}. The final catalyst layers for both electrodes contained 15 wt% Nafion®.

The anode polarization plot was obtained by converting the dry air gas at the cathode with H_2 to set the cathode up a dynamic hydrogen electrode (DHE) as well as a counter electrode. The anode potential was stepped from 0 to 1.25 V in 100 mV increments at 5 s intervals using a power supply (N5744A, Agilent). The H_2 gas was maintained at a rate of 400 sccm, while formic acid was supplied to the anode side of the test fuel cell at a flow rate of 5 ml min^{-1}.

RESULTS AND DISCUSSION

1. Physical Properties

Fig. 1 shows XRD patterns of the PdPtAu, Pd, Pt, and Au catalysts. Diffraction patterns indicate that the characteristic diffraction peaks of the PdPtAu catalyst were shifted to left and right as compared to those of Pt, Pd, and Au, respectively. It demonstrates

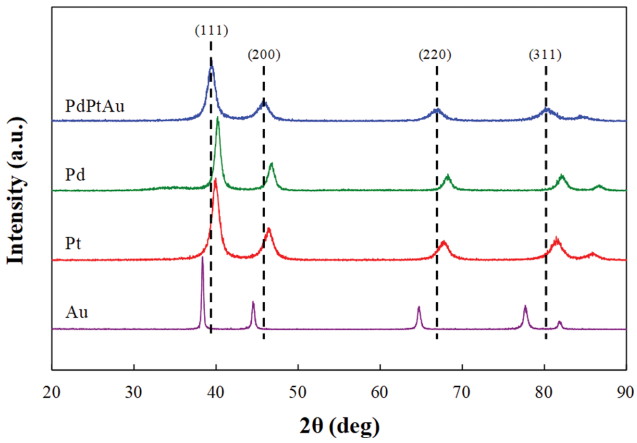

Fig. 1. XRD patterns of the PdPtAu, Pd, Pt, and Au catalysts.

Table 1. XRD and TEM results of Pt, Pd, Au, and PtPdAu catalysts

Catalysts	2θ (°)	d-Value	Lattice parameter (Å)[a]	Particle size	
				XRD[b]	TEM
PtPdAu	39.34	2.2884	3.9636	2.1	3.5
Pd	40.16	2.2435	3.8859	3.1	-
Pt	40.00	2.2522	3.901	3.1	-
Au	38.24	2.3517	4.0733	0.8	-

[a]Calculated from Pt(111) peak 2θ position according to Bragg formula.
[b]Calculated from Pt(111) peak using Debye-Scherrer equation

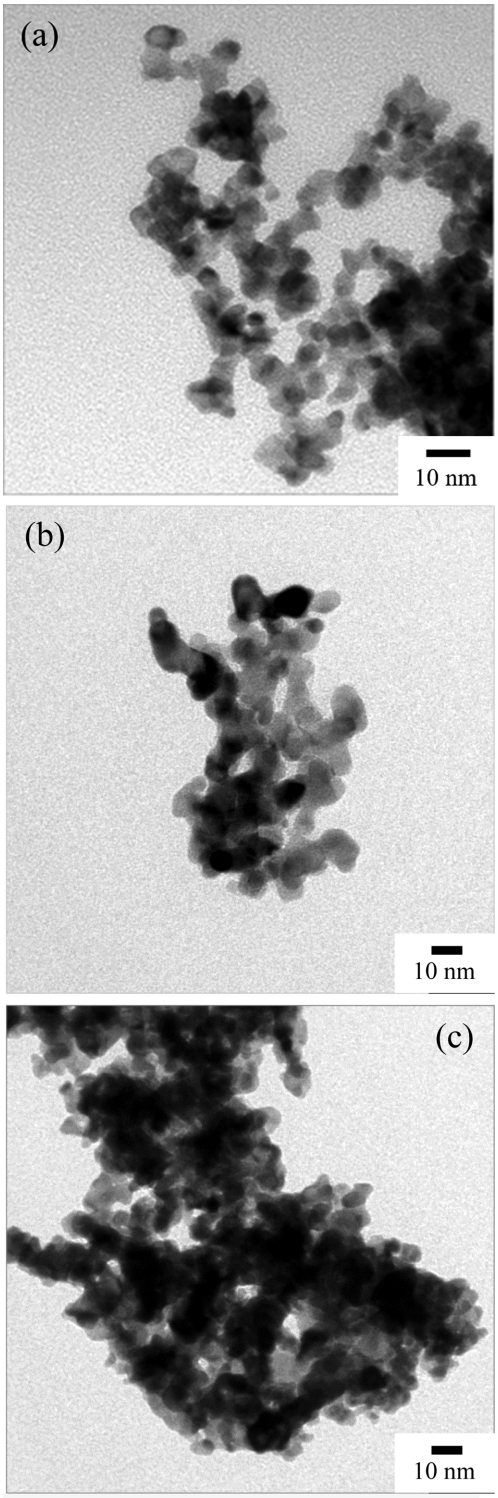

Fig. 2. TEM image of the (a) PdPtAu, (b) Pd, and (c) Pt catalysts.

clearly that the PdPtAu catalyst exhibited alloy formation and that the catalyst is a face-centered cubic (fcc) crystal. The mean particle size calculated by Debye-Scherrer equation was 2.1 nm, while ca. 3.5 nm was obtained by the TEM image analysis as shown in Fig. 2(a). For comparison, in Fig. 2(b) and (c), the Pd and Pt catalysts were shown and their particles are severely aggregated as compared to the PdPdAu catalyst. The physical properties assessed by XRD and TEM are summarized in Table 1.

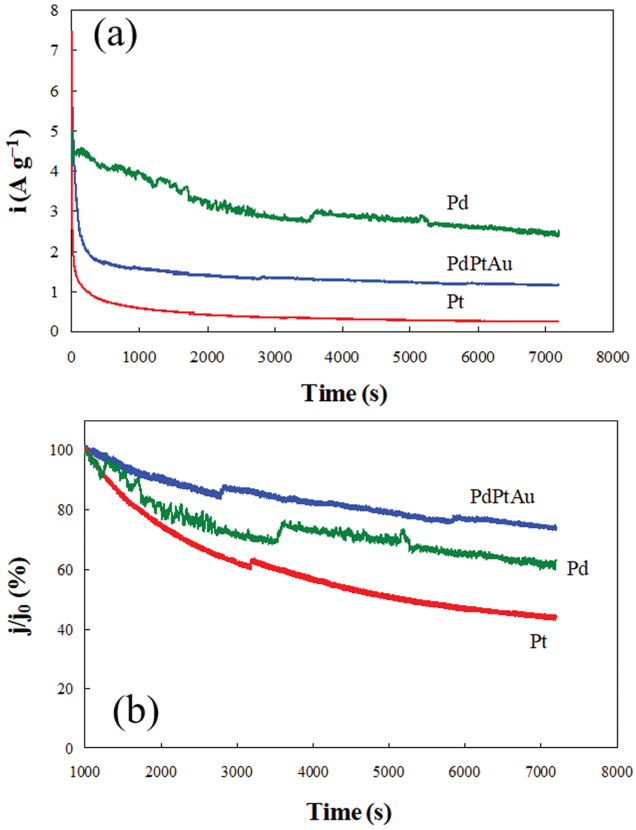

Fig. 3. (a) The chronoamperometric curves of 5 M HCOOH in 0.5 M H_2SO_4 solution at 0.1 V for 2 h at ambient temperature. (b) The deactivation degree as a function of time.

2. Electrochemical Properties

Fig. 3(a) exhibits the chronoamperometric curves of the Pt, Pd, and PdPtAu at a constant voltage of 0.1 V for 2 h at room temperature in 5 M HCOOH+0.5 M H_2SO_4 solution. In Fig. 3(a), we observed that the activity of the PdPtAu catalyst for formic acid oxidation was not as high as that of the Pd catalyst. However, it was higher than that of the Pt catalyst. For example, current per catalyst weight of the Pd, the PdPtAu, and Pt catalysts after 2 h-operation was 2.47, 1.15, and 0.25 A g^{-1}, respectively. To distinguish the deactivation degree among catalysts clearly, Fig. 3(b) was plotted according to Fig. 3(a) as follows:

$$\text{Deactivation degree (\%)} = \left(1 - \frac{j}{j_0}\right) \times 100\%$$

where j_0 is the current at 1,000 seconds to remove the initial unstable current and j is the current at the arbitrary time.

Fig. 3(b) indicates that the PdPtAu catalyst was more stable than the Pd and Pt catalysts for formic acid oxidation. After 2 h, the deactivation degree of PdPtAu, Pd, and Pt catalysts was 27%, 39%, and 57%, respectively.

Fig. 4 shows the pristine CV diagrams of PdPtAu, Pd, Pt, and Au catalysts obtained by normalizing with the total metal mass. The CV measurement was performed in 0.5 M H_2SO_4 solution at

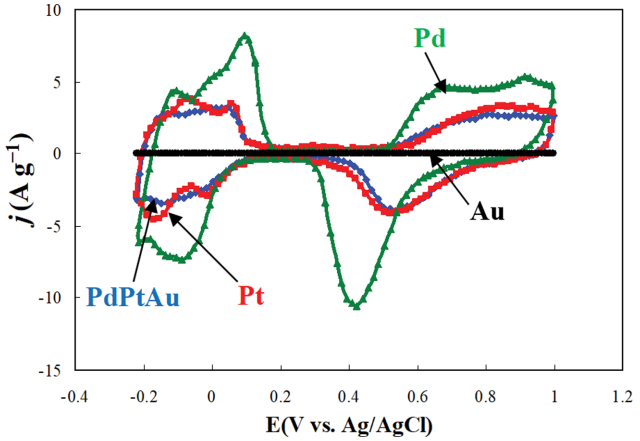

Fig. 4. Pristine CV diagrams of the PdPtAu, Pt, Pd, and Au catalysts in 0.5 M H_2SO_4 at ambient temperature.

the scan rate of 20 mV s^{-1}. First, the hydrogen adsorption and desorption regions for the Pt catalyst were placed between −0.2 V and 0.1 V. The peak around 0.7 V was attributed to the platinum oxide, while the region related to reduction was begun on 0.52 V approximately. For the Pd catalyst, the peaks corresponding to hydrogen adsorption/desorption are shown in a different range from the Pt catalyst. The regions of oxidation and reduction of hydrogen were observed between −0.22 and 0.2 V. For that reason, the double layer region of the Pd catalyst was suppressed as compared to that of the Pt catalyst. According to Fig. 4, it indicates that the Pd catalyst had more sites to adsorb hydrogen than the Pt catalyst. The Pd oxide was formed in about 50 mV lower potential than on the Pt catalyst. In contrast to Pd and Pt catalysts, the Au catalyst showed different electrochemical behavior in the full range. There was no significant peak of hydrogen or oxide formation on the Au catalyst as compared to other catalysts. The results are consistent with previous literature for formic acid oxidation [24,25]. According to their results, the electro-oxidation of the formic acid on the Au surface did not form poisoning species. The PdPtAu catalyst exhibited different patterns from the Pd and Pt catalysts. There were two peaks between −0.22 V and 0.1 V. Hydrogen adsorption or desorption peaks of the PdPtAu catalyst were similar to those of the Pt catalyst about the corresponding potential range. On the other hand, it was similar to the Pd catalyst that the current of the second peak was higher than that of the first peak. Surface oxides on the PdPtAu catalyst were formed less than on the Pd and Pt catalysts when comparing their oxidation current. We speculate that pores of the Pd catalyst were decreased while being alloyed. Also, we conjecture that the electrochemical property of the PdPtAu catalyst simulates the general propensity of the Pd, while the current of the PdPtAu catalyst is more diminished than that of the Pd catalyst. These characteristics caused higher activity than the Pt and less deactivated than the Pd catalyst as shown in Fig. 3.

3. Stripping Test of the Pd, Pt, and PdPtAu Catalysts

Fig. 5 shows the results of electrodes that were electrochemically stripped after being operated at 0.1 V for 2 h in 5 M HCOOH. After 2 h, electrodes were stripped from –0.22 V to 1.0 V in 0.5 M H_2SO_4 at ambient temperature. The scan rate was 20 mV s^{-1}. A sharp

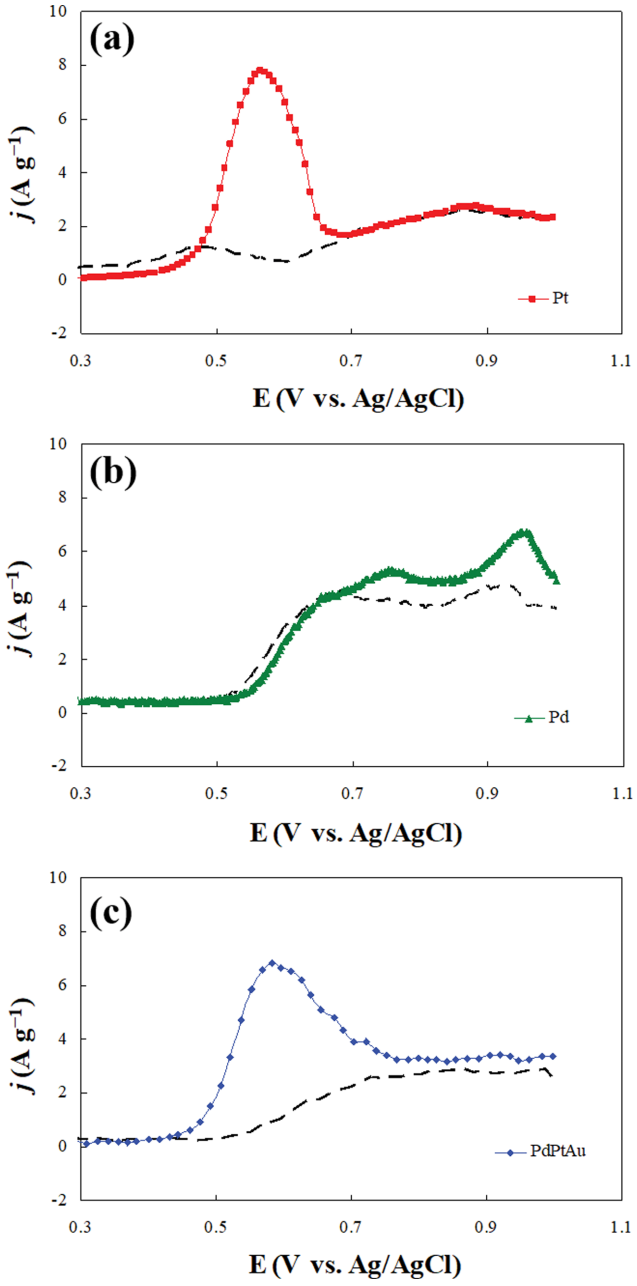

Fig. 5. Stripping voltammetry of the (a) Pt, (b) Pd, and (c) PdPtAu after applying the constant potential at 0.1 V in 5 M HCOOH for 2 h. The black dashed line is the pristine CV in 0.5 M H_2SO_4.

peak at 0.57 V related to the oxidation of CO_{ads} was observed in Pt catalyst (Fig. 5(a)) [26,27]. Except for the peak at 0.57 V, there was no peak on the Pt catalyst except for a CO_{ads} peak compared to the CV diagram in 0.5 M H_2SO_4. However, for the Pd catalyst, there were two apparent differences between before and after poisoning. The mass-specific current density at the first peak (at 0.76 V) related to CO_{ads} was lower than that produced by the Pt catalyst. According to the literature [28], we assume that this peak corresponds to the CO_{ads} formation, while the formic acid was oxidized via a similar pathway (2) with the Pt catalyst [29-31]. The second

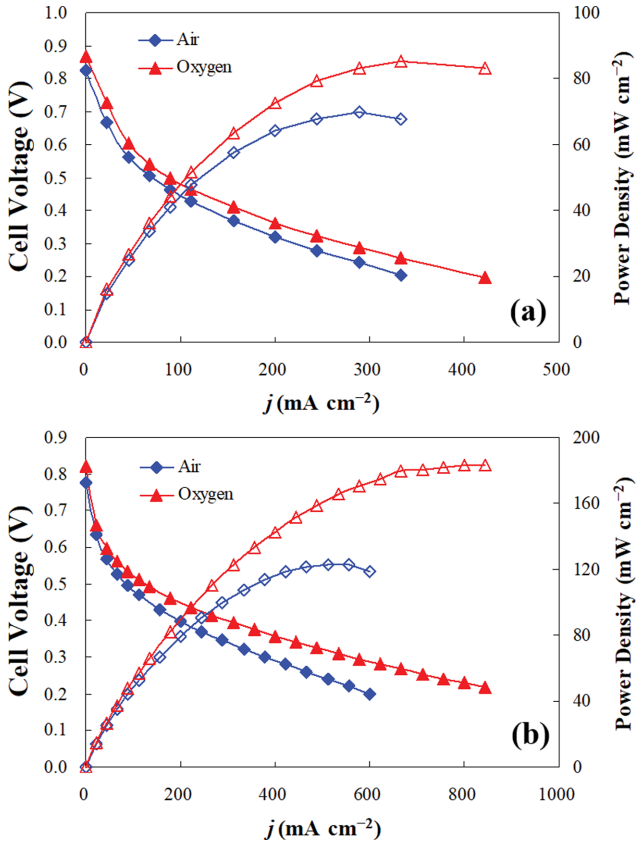

Fig. 6. The single cell performance of the PdPtAu anode at (a) 30 °C and (b) 60 °C. 5 M HCOOH was fed to the anode at the rate of 5 ml min^{-1}. Dry air and oxygen were supplied to the cathode at the rate of 800 sccm and 400 sccm. respectively.

peak undetected in the stripping voltammetry of the Pt catalyst was found in the potential of 0.95 V. The second peak showed higher mass-specific current density than CO_{ads}-related one. The increased mass-specific current density of CO_{ads} and non CO_{ads} species was 13% and 25% as compared to the one in the pristine CV, respectively. According to the result, the poisoning species other than CO might be a factor in terms of stability. In this work, the exact species was not identified. However, the formate might be a candidate for the poisoning species since the literature showed that the third reaction pathway so called "formate pathway" was proposed since the formate was detected by in-situ IR spectra [32]. The PdPtAu catalyst in Fig. 5(c) exhibits one peak as opposed to the Pd catalyst and that peak was observed at higher oxidation potential than the Pt catalyst.

4. MEA Tests

Fig. 6 shows the MEA performance of the PdPtAu and Pt black catalyst in the anode and cathode, respectively, at 30 and 60 °C. 5 M HCOOH was fed to the anode at a flow rate of 5 ml min^{-1} while the dry oxygen and air were supplied to the cathode at a flow rate of 400 sccm and 800 sccm, respectively. As the temperature increased, the open circuit voltage (OCV) was decreased by approximately 60 mV and 50 mV for the air and oxygen, respectively. It appeared since the mixed potential from the HCOOH crossover against Nafion® increased with the temperature [33]. As shown in Fig. 6,

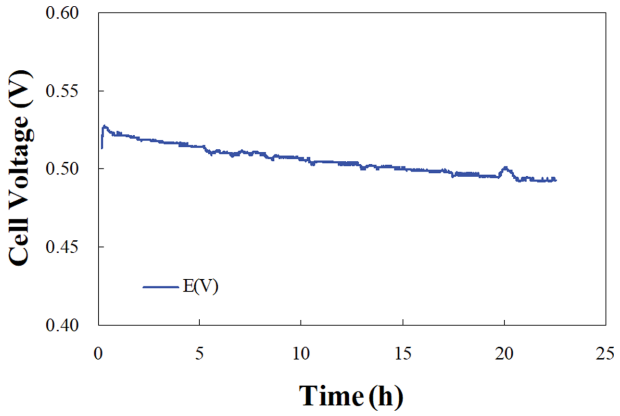

Fig. 7. Stability test of a single cell with PdPtAu-based anode for 23 h at 100 mA cm^{-2}. 5 M HCOOH and dry oxygen were fed to the anode and cathode at 60 °C, respectively.

the maximum power density of the PdPtAu catalyst exhibited ca. 85 and 180 mW cm^{-2} when dry oxygen was supplied at 30 and 60 °C, respectively.

Fig. 7 shows the stability of the PdPtAu catalyst used for the anode within 23 h at 100 mA cm^{-2}. 5 M formic acid and dry oxygen were supplied into the anode and cathode at the rate of 5 m min^{-1} and 400 sccm, respectively. The change of cell voltage was from 0.526 V to 0.496 V. the cell voltage loss of the single cell was 5.7% for 23 h of operation. It represents that although its catalytic activity is lower than the Pd's one, PdPtAu is an oxidative catalyst for the formic acid without strong deactivation despite a long time of operation. We expect that the Au can help the active Pd and Pt be more durable towards CO poisoning since the Au is known as a good catalyst for CO oxidation [34]. The reduction potential of the Au is higher than the Pd and Pt, which may result in the Au being reduced on the surface mostly. As a result, the CO oxidation would be efficient and durable on the PdPtAu as compared to the Pd catalyst. Also, the benefits from the alloying metals would be attributed to the enhanced durability since the alteration of electronic structure via the strain effect and the ligand effect affects the catalytic performance and durability [35-37]. The Pt binding site density was lowered and the formic acid oxidation took place via the direct pathway by alloying the Au, Pt, and Pd metals, which induced the enhanced CO resistance and performance [35,38-40].

CONCLUSIONS

The tri-metallic PdPtAu alloy by co-precipitation method is reported to reduce the degradation of the anodic catalyst. From experiments in an electrochemical cell, we conclude that the PdPtAu is well adjusted as an anodic catalyst for the DFAFCs. Although the mass-specific current density of the Pd catalyst is higher than that of the PdPtAu catalyst, two-fold enhancement of the catalytic reactivity of PdPtAu than that of the Pt is shown and the PdPtAu catalyst exhibits even better stability than Pd and Pt catalysts. In stripping tests, the Pd catalyst exhibited two different oxidation peaks, while one oxidation peak was shown for the Pt and PdPtAu catalysts. The MEA employed PdPtAu-based anode showed the maximum

power density of 180 mW cm^{-2} at 60 °C. Additionally, the long-term stability test showed a low voltage loss of 5.7% over 23 h. Those results indicate that the PdPtAu catalyst is a promising anodic catalyst for formic acid oxidation.

ACKNOWLEDGEMENTS

This work was supported by the Korea Institute of Science and Technology and the National Research Foundation of Korea (NRF) grant funded by the Korea government (MSIT) (No. 2020R1C1 C1004206).

REFERENCES

1. S. Ha, Z. Dunbar and R. I. Masel, *J. Power Sources*, **158**, 129 (2006).
2. S. Ha, R. Larsen and R. I. Masel, *J. Power Sources*, **144**, 28 (2005).
3. S. Ha, R. Larsen, Y. Zhu and R. I. Masel, *Fuel Cells*, **4**, 337 (2004).
4. W. S. Jung, J. Han and S. Ha, *J. Power Sources*, **173**, 53 (2007).
5. W. S. Jung, J. Han, S. P. Yoon, S. W. Nam, T.-H. Lim and S.-A. Hong, *J. Power Sources*, **196**, 4573 (2011).
6. S.-H. Uhm, H.-R. Jeon and J.-Y. Lee, *J. Electrochem. Sci. Technol.*, **1**, 10 (2010).
7. L. Sui, W. An, C. K. Rhee and S. H. Hur, *J. Electrochem. Sci. Technol.*, **11**, 84 (2020).
8. S. D. Han, J. H. Choi, S. Y. Noh, K. Park, S. K. Yoon and Y. W. Rhee, *Korean J. Chem. Eng.*, **26**, 1040 (2009).
9. Y. Wang, Z. Xiong and Y. Xia, *RSC Adv.*, **7**, 40462 (2017).
10. H. Shi, F. Liao, W. Zhu, C. Shao and M. Shao, *Int. J. Hydrogen Energy*, **45**, 16071 (2020).
11. S.-Y. Lee, N. Jung, J. Cho, H.-Y. Park, J. Ryu, I. Jang, H.-J. Kim, E. Cho, Y.-H. Park, H. C. Ham, J. H. Jang and S. J. Yoo, *ACS Catal.*, **4**, 2402 (2014).
12. D. Liu, M. Xie, C. Wang, L. Liao, L. Qiu, J. Ma, H. Huang, R. Long, J. Jiang and Y. Xiong, *Nano Res.*, **9**, 1590 (2016).
13. Y. Lu and W. Chen, *ACS Catal.*, **2**, 84 (2012).
14. H. Liao, J. Zhu and Y. Hou, *Nanoscale*, **6**, 1049 (2014).
15. L. Hong, Q. Dong, Q. Qin, H. Li, J. Xie, G. Yu and H. Chen, *Int. J. Hydrogen Energy*, **44**, 19900 (2019).
16. L. Y. Zhang, Y. Gong, D. Wu, Z. Li, Q. Li, L. Zheng and W. Chen, *Appl. Surf. Sci.*, **469**, 305 (2019).
17. A. Shafaei Douk, H. Saravani and M. Noroozifar, *J. Alloys Compd.*, **739**, 882 (2018).
18. L. Juárez-Marmolejo, S. Pérez-Rodríguez, M. G. Montes de Oca-Yemha, M. Palomar-Pardavé, M. Romero-Romo, A. Ezeta-Mejía, P. Morales-Gil, M. V. Martínez-Huerta and M. J. Lázaro, *Int. J. Hydrogen Energy*, **44**, 1640 (2019).
19. Y. Jin, J. Zhao, F. Li, W. Jia, D. Liang, H. Chen, R. Li, J. Hu, J. Ni, T. Wu and D. Zhong, *Electrochim. Acta*, **220**, 83 (2016).
20. K. Ding, L. Liu, Y. Cao, X. Yan, H. Wei and Z. Guo, *Int. J. Hydrogen Energy*, **39**, 7326 (2014).
21. A. Caglar, B. Ulas, M. S. Cogenli, A. B. Yurtcan and H. Kivrak, *J. Electroanal. Chem.*, **850**, 113402 (2019).
22. C. Xu, Q. Hao and H. Duan, *J. Mater. Chem. A*, **2**, 8875 (2014).
23. Y. Li, X. Cao, L. Wang, Y. Wang, Q. Xu and Q. Li, *J. Taiwan Inst. Chem. Eng.*, **76**, 109 (2017).
24. J.-H. Choi, K.-W. Park, I.-S. Park, K. Kim, J.-S. Lee and Y.-E. Sung, *J. Electrochem. Soc.*, **153**, A1812 (2006).
25. T. J. Schmidt, H. A. Gasteiger, G. D. Stäb, P. M. Urban, D. M. Kolb and R. J. Behm, *J. Electrochem. Soc.*, **145**, 2354 (1998).
26. G.-Q. Lu, A. Crown and A. Wieckowski, *J. Phys. Chem. B*, **103**, 9700 (1999).
27. S. Wasmus, D. A. Tryk and W. Vielstich, *J. Electroanal. Chem.*, **377**, 205 (1994).
28. W. P. Zhou, A. Lewera, R. Larsen, R. I. Masel, P. S. Bagus and A. Wieckowski, *J. Phys. Chem. B*, **110**, 13393 (2006).
29. A. Capon and R. Parsons, *J. Electroanal. Chem. Interfacial Electrochem.*, **44**, 1 (1973).
30. A. Capon and R. Parsons, *J. Electroanal. Chem. Interfacial Electrochem.*, **45**, 205 (1973).
31. A. Capon and R. Parsons, *J. Electroanal. Chem. Interfacial Electrochem.*, **44**, 239 (1973).
32. Y. X. Chen, M. Heinen, Z. Jusys and R. J. Behm, *Angew. Chem. Int. Ed.*, **45**, 981 (2006).
33. K.-J. Jeong, C. M. Miesse, J.-H. Choi, J. Lee, J. Han, S. P. Yoon, S. W. Nam, T.-H. Lim and T. G. Lee, *J. Power Sources*, **168**, 119 (2007).
34. H. Ha, S. Yoon, K. An and H. Y. Kim, *ACS Catal.*, **8**, 11491 (2018).
35. B. Ulas, A. Caglar, A. Kivrak, N. Aktas and H. Kivrak, *Ionics*, **26**, 3109 (2020).
36. W. S. Jung, W. H. Lee, H.-S. Oh and B. N. Popov, *J. Mater. Chem. A*, **8**, 19833 (2020).
37. W. S. Jung and B. N. Popov, *ACS Appl. Mater. Interfaces*, **9**, 23679 (2017).
38. J. Huang, H. Hou and T. You, *Electrochem. Commun.*, **11**, 1281 (2009).
39. K. Jiang, H.-X. Zhang, S. Zou and W.-B. Cai, *PCCP*, **16**, 20360 (2014).
40. X. Gu, Z.-H. Lu, H.-L. Jiang, T. Akita and Q. Xu, *J. Am. Chem. Soc.*, **133**, 11822 (2011).